A Portable Ka-Band Front-End Test Package for Beam-Waveguide Antenna Performance Evaluation—Part II: Tests on the Antenna

T. Y. Otoshi, S. R. Stewart, and M. M. Franco
Ground Antennas and Facilities Engineering Section

In "Part I" of this article, a description was given of a Ka-band test package developed to enable testing of the new DSS 13 34-m beam-waveguide (BWG) antenna at 32 GHz. Test results were given for the Ka-band test package in an "on-the-ground" test configuration. This article, "Part II," is a companion article concerned with Ka-band test results for the test package in an "on-the-antenna" test configuration. Included are Ka-band zenith noise-temperature values, tipping-curve data, and subreflector test results obtained at the Cassegrain focal point F1, as well as at the final BWG focal point F3 (located in a subterranean pedestal room). Test results show that, through the use of the Ka-band test package, the BWG antenna performance was successfully evaluated at Ka-band. The Ka-band test package operated well in all of the different antenna test configurations.

I. Introduction

As described in [1], a new 34-m beam-waveguide (BWG) antenna has been built at Deep Space Station 13 in the Deep Space Communications Complex at Goldstone, near Barstow, California. This new antenna is the first of the NASA tracking antennas to use a BWG design. A recent photograph of the newly constructed antenna is shown in Fig. 1. Figure 2 shows the various focal points (F1, F2, and F3) of the center-pass mode of this new BWG antenna. The experimental test program includes testing the new antenna at X-band (8.45 GHz), Ku-band (12 GHz), and Ka-band (32 GHz).

As described in previous reports [1,2], a unique methodology was used to test the new antenna at the different frequency bands. The methodology involved the use of portable test packages that could be transported to the various focal points (see Fig. 2). Measurements of operating noise temperatures and antenna efficiencies were made as functions of antenna elevation and azimuth angles at the different focal points of the BWG antenna. Comparisons of data measured at the different focal points enabled determinations of the performance degradations caused by various mirrors in the BWG system.

Previous reports [1,2] gave results of X-band test package measurements in "on-the-ground" and "on-the-antenna" test configurations. The results of Ka-band test package measurements in an on-the-ground test configuration were presented in a companion article, "Part I," in this issue [3].

This present article, "Part II," is the fourth of a series of reports on the results of measurements obtained through the use of portable microwave test packages to evaluate the performance of the new BWG antenna. Presented in this article are Ka-band zenith operating noise temperatures measured at focal points F1, F2, and F3, as well as Ka-band tipping curve and subreflector test data. Beam-waveguide antenna efficiencies measured with the X- and Ka-band test packages at F1 and F3 are presented in another article in this issue [4]. Another related article in this issue is concerned with the BWG antenna-pointing data obtained with the X- and Ka-band test packages [5].

II. Installations

Figure 3 shows the Ka-band 29-dBi horn test package installed on the antenna at the Casssegrain focal point F1. The structure shown supporting the Ka-band test package is a universal F1 mounting assembly that allows any of the three 29-dBi horn configuration test packages (X- ,Ku-, or Ka-band) to be interchanged and installed.

After completing measurements of noise temperature and antenna efficiencies at F1, the Ka-band test package was removed and then reconfigured to a 23-dBi horn configuration and installed at F3 (Fig. 4). The mounting table shown is a universal F3 mounting assembly that can support any of the test packages (X-, Ku-, or Ka-band) and provides three-axis adjustment of the test package location. Adjustments of ± 3 in. can be made along three orthogonal axes (i.e., the vertical direction, the radial direction towards and away from the BWG hub center, and the other transverse direction).

III. Test Results

A. Zenith Operating Noise-Temperature Measurements

Figure 5 shows plots of gain factor, linearity, and operating noise temperatures when the 29-dBi horn test package was mounted at F1. Figure 5(a) shows that over the 16-hour test period, the gain factor varied from 0.999 to 0.993, corresponding to a peak-to-peak gain change of only 0.03 dB. Figure 5(b) shows that during this same test period, the change in operating noise temperature was approximately 0.6 K peak-to-peak.

Figure 6 shows typical plots obtained when the test package was mounted at F3. Over a 14-hour period, the gain factor varied from 0.995 to 1.005, corresponding to a peak-to-peak gain change of about 0.04 dB. The change in operating noise temperature was approximately 0.8 K peak-to-peak.

It was fortuitous that Ka-band tests were done during winter months when the weather was cold and the humidity low. As may be seen in Figs. 5(b) and 6(b), the operating noise temperatures were reasonably constant for tests at both F1 and F3. It should be pointed out that in these plots, the ambient-load physical temperatures are correlated with the outside air temperatures at F1 (an outdoor environment), but uncorrelated when the test package is at F3 (an indoor environment). At Ka-band, operating noise-temperature values are very sensitive not only to outside air temperature and relative humidity, but also to variable cloud cover, atmospheric inversion layers, and uneven heating of the atmosphere.

For the operating noise-temperature values shown in Figs. 5(b) and 6(b), corrections were made for gain changes, but not for nonlinearity, which was typically less than 1 percent. Since the uncertainty of the linearity corrections are themselves about ± 1 percent, the small linearity corrections, if made, would not significantly enhance the quality of the operating noise-temperature data shown on these particular plots.

A summary of results of Ka-band zenith operating noise temperatures for the ground and F1, F2, and F3 locations is given in Table 1. The value shown in the table for each test configuration is the grand average of the average operating noise temperatures determined for the individual observing periods. The total span of time over which observations were made is about four months. Each grand average value shown in Table 1 is estimated to have an uncertainty of ± 1.5 K (one standard deviation).

Zenith operating noise temperatures for the F2 focal point were extrapolated from antenna tipping-curve tests and from a star track. Therefore, the confidence level of the data at F2 is not as high as at the other focal point locations where more data were obtained. Tests were done at F2 for diagnostic purposes to investigate a "hysteresis-like" characteristic on antenna efficiency measurements. The value obtained at F2 is included in Table 1 to enable interesting comparisons with values obtained at other focal points.

One of the primary goals of the experiment was to determine the amount of BWG antenna degradations caused by the mirror system. The methodology proposed to determine the degradations was to take the difference of values obtained at the various focal points. Table 2 shows differential noise temperatures for the various configurations. The "F1 – ground" configuration data have a value of 7.1 K due primarily to scattering from the subreflector and tripod, leakage through the main reflector surface,

and spillover from the main reflector. Another cause of noise temperature increase at F1 is a temporary perforated plate having 3/8-in.-diameter holes was used to cover the bypass shroud opening (Fig. 3) on the main reflector surface. Even though this plate is reflective at X-band, it begins to approach transparency at Ka-band frequencies. The ground noise contributions due to leakage through this perforated plate are, therefore, greater at 32 GHz than at 8.45 GHz. The amount of noise contribution might be estimated from information provided in [2] for the shroud opening (when uncovered) at 8.45 GHz. More noise might also have been contributed by numerous pieces of masking tape (Fig. 3) covering panel-adjustment bolt holes on the main reflector surface. The numerous pieces of masking tape, used to post panel-adjust information, were not removed after completing holography measurements at F1. Although the masking tape pieces might not have affected holography or X-band measurements, they might have increased reflector surface noise temperature contributions at Ka-band.

Comparisons of the "F3 - F1" values before and after mirror realignments show that realignment of the mirrors resulted in a lowering of the operating noise temperature by 3.8 K. The final "F3 - F1" value of 6.8 K provides a realistic measure of the degradation caused by six mirrors (including the ellipsoid) of the BWG system.

Table 3 is a worksheet showing how the final values summarized in Table 1 were derived. Shown are the observation periods, the measured operating noise-temperature values, weather information, and normalized values after corrections were made for weather and waveguide physical temperatures. In Table 3, the normalized T_{op} was computed from

$$T_{op,n} = T_{op} + \frac{T'_{cb}}{L_{wg}}\left(\frac{1}{L_{atm,s}} - \frac{1}{L_{atm}}\right) + \frac{1}{L_{wg}}(T_{atm,s} - T_{atm}) + (T_{wg,s} - T_{wg}) \quad (1)$$

where T_{op}, T_{atm}, T_{wg}, and L_{atm} are, respectively, the average measured T_{op}, computed T_{atm}, T_{wg}, and L_{atm} values given in Table 4, and where other noise-temperature symbols are defined in Table 1 of "Part I" [3]. The Ka-band (32.0 GHz) values used in Eq. (1) were T'_{cb} = 2.0 K [3], $T_{atm,s}$ = 7.02 K (for a Goldstone average clear atmosphere[1]), $L_{atm,s}$ = 1.02683 (corresponding to 0.1150 dB), L_{wg} = 1.06414 (corresponding to 0.27 dB), $T_{wg,s}$ = 17.67 K for the above L_{wg}, and a standard physical waveguide temperature of 20 deg C.

At Ka-band and higher microwave frequencies, weather changes can cause significant variations in the atmospheric noise contributions to the operating noise temperatures. In "Part I" [3], curves were presented showing that at Ka-band, typical weather conditions at DSS 13 during the year can cause the atmospheric noise temperatures to vary from 4.5 to 31.2 K, which represents a peak-to-peak variation of about 27 K. As may be seen in Table 3, the applications of weather corrections enabled significant improvements to be made in the comparisons of operating noise temperatures for the different test configurations—even when the measurements were performed on different days or months of different test configurations.

B. Cassegrain and BWG Antenna Loss Factors

It is of interest to determine equivalent loss factors for the BWG system. Stelzried and Otoshi [6] have shown that loss factors of very low-loss antenna waveguide components can sometimes be determined from radiometric methods when it is not possible to use conventional insertion-loss measurement techniques.

The derivations of the equations for BWG-antenna loss factors are straightforward, but lengthy, and will not be presented here. However, the basic equations needed to derive the loss factor equations will be presented. Let L_{F1} be defined as the loss factor associated with dissipative losses at the Cassegrain reflector surface, L_{F2} the loss factor of the BWG section between F1 and F2, and L_{F3} the loss factor of the BWG section between F1 and F3. The following basic equations apply for the measurements made with the test packages:

$$T_{sky} = \frac{T'_{cb}}{L_{atm}} + T_{atm} \quad (2)$$

$$T_{tp} = T_{wg} + T_{hemt} + T_{fu} \quad (3)$$

$$T_{op,g} = \frac{T_{sky}}{L_{wg}} + T_{tp} \quad (4)$$

$$T_{bwg,F1} = \left(1 - \frac{1}{L_{F1}}\right) T_p \quad (5)$$

$$T_{bwg,F2} = \left(1 - \frac{1}{L_{F2}}\right) T_p \quad (6)$$

[1] *Deep Space Network/Flight Project Interface Design Handbook*, Document 810-5, Rev. D, vol. I, sec. TCI-30 (internal document), Jet Propulsion Laboratory, Pasadena, California, June 1, 1990.

$$T_{bwg,F3} = \left(1 - \frac{1}{L_{F3}}\right) T_p \tag{7}$$

$$T_p = 20 + 273.16 = 293.16 \text{ K} \tag{8}$$

$$T_{op,F1} = \frac{T_{sky}}{L_{F1} L_{wg}} + \frac{T_{bwg,F1}}{L_{wg}} + T_{tp} \tag{9}$$

$$T_{op,F2} = \frac{T_{sky}}{L_{F1} L_{F2} L_{wg}} + \frac{T_{bwg,F1}}{L_{F2} L_{wg}} + \frac{T_{bwg,F2}}{L_{wg}} + T_{tp} \tag{10}$$

$$T_{op,F3} = \frac{T_{sky}}{L_{F1} L_{F3} L_{wg}} + \frac{T_{bwg,F1}}{L_{F3} L_{wg}} + \frac{T_{bwg,F3}}{L_{wg}} + T_{tp} \tag{11}$$

Substitutions of Eqs. (2) through (8) into Eqs. (9) through (11) and algebraic manipulations lead to the loss factor expressions of

$$L_{F1} = \frac{1}{1 - \left[\dfrac{L_{wg}(\Delta T_{op})_{1g}}{T_p - T_{sky}}\right]} \tag{12}$$

$$L_{Fj} = \frac{1}{1 - \left[\dfrac{L_{F1} L_{wg} (\Delta T_{op})_{j1}}{T_p - T_{sky}}\right]} \tag{13}$$

where $j = 2$ or 3. The expressions for the differential operating noise temperatures are

$$(\Delta T_{op})_{1g} = T_{op,F1} - T_{op,g} \tag{14}$$

$$(\Delta T_{op})_{21} = T_{op,F2} - T_{op,F1} \tag{15}$$

$$(\Delta T_{op})_{31} = T_{op,F3} - T_{op,F1} \tag{16}$$

The above loss factor equations are functions of elevation angle, but measured T_{op} values are generally only available for the zenith test configuration. The following example is given for a zenith test configuration. Substitutions of Table 2 and Eq. (1) values into the above equations result in $L_{F1} = 1.02732$ (Cassegrain reflector associated dissipative losses), $L_{F2} = 1.0204$ (for BWG dissipative losses between F1 and F2), $L_{F3} = 1.04251$ (for BWG dissipative losses between F1 and F3, for F3 before mirror realignment), and $L_{F3} = 1.02686$ (for BWG dissipative losses between F1 and F3, for F3 after mirror realignment). As will be demonstrated in the following section, the above loss factors are useful for extracting the atmospheric noise temperatures from tipping-curve data obtained at the various BWG focal points.

C. Tipping Curves

Tipping-curve tests were performed at F1, F2, and F3 at various azimuth angles for the test package. A few of the tipping curves are shown in Fig. 7. Most of the tipping-curve data at 32 GHz were obtained at an azimuth angle of 50 deg, because, at this azimuth, the ground is at a very low (1-deg) elevation angle. For most large antennas in the DSN, it has not been possible to accurately extract atmospheric noise temperatures from tipping-curve data. However, it was reported in [2] that it was possible to extract X-band atmospheric values from tipping curves that agreed with theoretical values to ±0.2 K. A plausible explanation for this good agreement is the low scattering cross-sections of the newly designed slim tripod legs on this new BWG antenna.

For a flat-Earth model, the equation for extracting the zenith atmospheric noise temperature from tipping-curve data is derived as

$$T_{atmz} = L_{ant} \left[\frac{T_{op}(\psi_{el}) - T_{op}(90)}{\dfrac{1}{\sin(\psi_{el})} - 1}\right] + T'_{cb}\left(1 - \frac{1}{L_{atmz}}\right) \tag{17}$$

where

ψ_{el} = the elevation angle, deg

$T_{op}(\psi_{el})$ = the operating system temperature measured at ψ_{el}, K

$T_{op}(90)$ = the operating system temperature measured at $\psi_{el} = 90$ deg or at zenith, K

L_{atmz} = the loss factor for the zenith atmosphere. An estimate of this value can be made by using the loss factor for a standard atmosphere, or a better estimate can be obtained by using the SDSATM7M.BAS program[2]

T'_{cb} = the effective contribution to T_{op} from the cosmic background, K

L_{ant} = the loss factor from the Cassegrain antenna aperture to the input to the HEMT, K

[2] Courtesy of S. Slobin of the Jet Propulsion Laboratory, Pasadena, California. SDSATM7M.BAS is a modified version of SDSATM4.BAS, but gives the same answers.

The above equation should not be used for ψ_{el} values close to 90 deg or less than 10 deg. In practice, it has been found that Eq. (17) is most accurate when used with tipping-curve data in the region of a 30-deg elevation angle. For the special case of $\psi_{el} = 30$ deg, Eq. (17) becomes

$$T_{atmz} = L_{ant}[T_{op}(30) - T_{op}(90)] + T'_{cb}\left(1 - \frac{1}{L_{atmz}}\right) \quad (18)$$

At 32.0 GHz and under clear Goldstone Ka-band atmosphere conditions, the last term contributes only 0.05 K. For this BWG antenna, values of L_{ant} were calculated from values of L_{F1}, L_{F2}, L_{F3}, and L_{wg} given previously in Eqs. (12) and (13) and the following equations:

$$\text{For F1}: \quad L_{ant} = L_{F1}L_{wg} \quad (19)$$

$$\text{For F2}: \quad L_{ant} = L_{F1}L_{F2}L_{wg} \quad (20)$$

$$\text{For F3}: \quad L_{ant} = L_{F1}L_{F3}L_{wg} \quad (21)$$

Substitution of values already presented in this article into Eqs. (19) through (21) gives: for F1, $L_{ant} = 1.09322$ (corresponding to 0.387 dB); for F2, $L_{ant} = 1.1155$ (corresponding to 0.475 dB); for F3 before mirror realignment, $L_{ant} = 1.1397$ (corresponding to 0.568 dB); and for F3 after mirror realignment, $L_{ant} = 1.1226$ (corresponding to 0.502 dB).

The reader is reminded that the L_{ant} values for the various focal points all contain the Cassegrain reflector loss factor $L_{F1} = 1.02732$ (corresponding to 0.117 dB) and $L_{wg} = 1.06414$ (corresponding to 0.27 dB). For the above values of L_{ant}, it was assumed that the antenna associated loss factors do not change significantly between zenith and 30-deg elevation angles, and therefore, the values for these loss factors could be derived from zenith conditions. For more accuracy, the dependence of these loss factors on elevation angle might have to be considered.

Table 4 is a worksheet showing the methodology used to extract atmospheric noise contributions from operating noise temperatures measured at zenith and 30-deg elevation angles at the various BWG focal points. Also shown is a comparison of the measured T_{atm} as obtained through the use of Eq. (18) with the computed T_{atm} as obtained through the SDSATM7M.BAS program, which is based on the weather data shown. Analysis of the results in Table 4 will show that the measured atmospheric values at 32 GHz are higher that the computed values by 2.4 + 0.5/–0.7 K.

For interest, the more rigorous method given by Eqs. (12), (13), (19), (20), and (21) was also used to extract X-band atmospheric noise temperatures from tipping curve data reported in [2]. It was found that the agreement between measured values and computed values at 8.45 GHz is now +0.1/–0.3 K, instead of the ±0.2 K deviations reported previously [2].

The tipping-curve results at X- and Ka-band indicate that either: (1) The theoretical weather model at Ka-band is not as good as at X-band for predicting atmospheric contributions from weather data, or (2) the tipping-curve data at Ka-band is corrupted more than at X-band by elevation-angle-dependent noise contributions from tripod leg scattering, subreflector spillover, main reflector spillover, and leakage through the antenna panels.

D. Subreflector Tests

Figure 8 shows a Ka-band subreflector defocus curve measured at F1 at an average elevation angle of 45 deg. To obtain this curve, the antenna tracked radio source 3C274, which had a source noise temperature of about 2.2 K at 32 GHz. Measurements of operating noise temperatures were made as functions of subreflector defocus positions. The Ka-band antenna-pointing model computer program was relied upon to keep the peak of the antenna beam pointed at the radio source. At the time the F1 subreflector curve measurements were made, a good experimental procedure had not yet been developed and, therefore, the experimental data are not very good for the sidelobe regions or for the main beam below −10 dB. However, it can be seen that over most of the main beam of the subreflector defocus curve, good agreement is obtained between a theoretical model and the experimental curve. The theoretical curve is based on a Geometric-Theory-of-Diffraction/Jacobi-Bessel antenna program.[3]

Figure 9 shows subreflector data measured at F3 for an average elevation angle of 45 deg. To obtain this curve, the antenna tracked radio source 3C84, which had a source noise temperature of about 4 K at 32 GHz at the time of these tests. To obtain data for this experimental curve, an improved test procedure was developed and implemented. Boresight measurements were performed more often (at least twice) during the subreflector test, which took about

[3] P. Cramer, "Calculated DSS-13 Subreflector Z-Axis Focus Curves, Feed at F1," Interoffice Memorandum 3328-90-0355 (internal document), Jet Propulsion Laboratory, Pasadena, California, September 20, 1990.

two hours to perform. Sufficient numbers of off-source and on-source measurements were taken to allow for corrections of measurement system drifts. Also shown in Fig. 9 is a theoretical defocus curve for 32 GHz and a 45-deg rigging angle. It can be seen in Fig. 10 that good agreement was obtained between Cramer predictions and the experimental data down to about −15 dB for the main beam. Good agreement was also obtained for some regions of the sidelobe patterns.

It should be pointed out that even though Cramer's predictions were made for F1 and the experimental results in Fig. 9 are for F3, there is reasonably good agreement between theory and experiment. For a properly designed and aligned BWG mirror system, the subreflector defocus gain curves at F3 should be nearly identical to those at F1. Therefore, a Z-defocus subreflector test at F3 provides a good method for verifying the integrity of the BWG system.

A Z-defocus subreflector test is also useful for revealing whether multipath signals exist within a large antenna system [7,8]. Scrutiny of the subreflector defocus data near the peak of the main beam (Fig. 10) indicates no unusual humps. The absence of humps and ripples on the main-beam defocus curve shown in Fig. 10 indicates that the magnitudes of any multipath signals within the BWG system are small (for a 100-MHz bandwidth measurement).

To obtain accurate subreflector defocus data below the 20-dB level (Fig. 9) while tracking a 4 K source, the radiometer needs to provide resolutions and accuracies of better than 0.04 K. In addition, the Ka-band antenna-pointing model should be good enough to allow blind pointing and remain on the peak of the source to within ±2 mdeg.

E. Overall Performance

The overall performance characteristics of the Ka-band test package are summarized in Table 5. The performance data are based on observed test data in a worst-case field environment, as well as on error analyses equations given in the Appendix to "Part I" [3] and also [9]. Examination of Table 5 reveals that the Ka-band test package performance was good in terms of resolution, gain stability, and linearity.

The test package was subjected not only to mechanical stresses during radio source tracking at various elevation angles at F1, but also to ambient temperatures ranging from 0 to 40 deg C and transportation to and from the ground locations F1, F2, and F3 several times. Test data in Table 1 showed that the long-term stability and repeatability of data for the various test configurations were very good.

IV. Concluding Remarks

The objective of determining the amount of degradations due to the BWG mirrors has been met. The Ka-band test package operated well in all of the different test configurations. Zenith operating noise temperatures, tipping-curve data, and subreflector defocus curves were successfully obtained at F1 and F3. As reported elsewhere, the Ka-band test package also enabled high-quality and reliable data to be obtained for antenna efficiency and antenna-pointing tests.

Acknowledgments

The assistance of J. Garnica, G. Bury, J. Crook, G. Farner, R. Littlefair, and R. Reese, all of DSS 13, is gratefully acknowledged. The authors also thank DSS 13 Group Supervisor, C. Goodson, and the DSS 13 Station Manager, A. Price, for their quick responses and superb management support for tasks involving special tests of the X- and Ka-band test packages.

References

[1] T. Y. Otoshi, S. R. Stewart, and M. M. Franco, "A Portable X-band Front-End Test Package for Beam-Waveguide Antenna Performance Evaluation—Part I: Design and Ground Tests," *TDA Progress Report 42-103*, vol. July–September 1990, Jet Propulsion Laboratory, Pasadena, California, pp. 135–150, November 15, 1990.

[2] T. Y. Otoshi, S. R. Stewart, and M. M. Franco, "A Portable X-band Front-End Test Package for Beam-Waveguide Antenna Performance Evaluation—Part II: Tests on the Antenna," *TDA Progress Report 42-105*, vol. January–March 1991, Jet Propulsion Laboratory, Pasadena, California, pp. 54–68, May 15, 1991.

[3] T. Y. Otoshi, S. R. Stewart, and M. M. Franco, "A Portable Ka-band Front-End Test Package for Beam-Waveguide Antenna Performance Evaluation—Part I: Design and Ground Tests," *TDA Progress Report 42-106*, vol. April–May 1991, Jet Propulsion Laboratory, Pasadena, California, pp. 249–265, August 15, 1991.

[4] S. D. Slobin, T. Y. Otoshi, M. J. Britcliffe, L. S. Alvarez, S. R. Stewart, and M. M. Franco, "Efficiency Calibration of the DSS 13 34-Meter-Diameter Beam Waveguide Antenna at 8.45 and 32 GHz," *TDA Progress Report 42-106*, vol. April–May 1991, Jet Propulsion Laboratory, Pasadena, California, pp. 283–297, August 15, 1991.

[5] L. S. Alvarez, "Initial Pointing Calibrations for the DSS 13 34-Meter Beam-Waveguide Antenna," *TDA Progress Report 42-106*, vol. April–May 1991, Jet Propulsion Laboratory, Pasadena, California, pp. 188–204, August 15, 1991.

[6] C. T. Stelzried and T. Y. Otoshi, "Radiometric Evaluation of Antenna-Feed Component Losses," *IEEE Transactions on Instrumentation and Measurement*, vol. IM-18, no. 3, pp. 172–183, September 1969.

[7] G. S. Levy, D. A. Bathker, A. C. Ludwig, D. E. Neff, and B. L. Seidel, "Lunar Range Radiation Patterns of a 210-ft Antenna at S-band," *IEEE Transactions on Antennas and Propagation*, vol. AP-15, no. 2, pp. 311–313, March 1967.

[8] T. Y. Otoshi, "Multipath Tests on 64-m Antennas Using the Viking Orbiter-1 and -2 Spacecraft as Far-Field Illuminators," *DSN Progress Report 42-31*, Jet Propulsion Laboratory, Pasadena, California, pp. 41–49, February 15, 1976.

[9] C. T. Stelzried, "Operating Noise-Temperature Calibrations of Low-Noise Receiving Systems," *Microwave Journal*, vol. 14, no. 6, pp. 41–46 and 48, June 1971.

Table 1. Summary of Ka-band zenith operating noise temperatures at DSS 13 from October 12, 1990, through January 31, 1991

Config.	Observation Dates	Grand Average[a] T_{op}, K	Peak Deviations From Grand Avg., K
Ground	10/12/90, 11/09/90, 01/19/91, 01/31/91	84.7[b]	+1.6 −1.7
F1	10/13/90, 10/14/90, 01/11/91	91.8	+0.4 −0.6
F2	01/16/91, 01/17/91	97.0[c]	+0.4 −0.4
F3	11/10/90, 12/18/90	102.4	+0.1 −0.0
After mirrors and ellipsoid realigned on December 18, 1990			
F3	01/23/91, 01/25/91, 01/30/91	98.6[d]	+0.8 −0.7

[a] Normalized T_{op} values were computed through the use of Eq. (1).

[b] Ground values were reported in "Part I" [3]. The measured ground value of 84.7 K agrees closely with the predicted value of 84.5 K under standard conditions.

[c] No calibrations longer than 10 min were done at F2 with the antenna left at zenith.

[d] This number cannot be compared with the above F2 value. It is probable that the new F2 value is also lower after the mirror realignment, but a measurement was not made.

Table 2. Differential zenith operating noise temperatures for various test configurations at 32 GHz

Configurations Differenced	ΔT_{op}, K
F1 − Ground	7.1
F2 − F1	5.2
F3 − F1	10.6
After mirrors and ellipsoid realigned on December 18, 1990	
F3 − F1	6.8

Notes: See Table 1 for F1, F2, and F3 values.

Do not compare the values for F3 − F1 after December 18, 1990, with the value for F2 − F1, because the value at F2 might have become lower, but was not remeasured.

Table 3. Ka-band (32 GHz) measured zenith operating noise temperatures corrected for weather and waveguide noise changes

Config.	Observation Period	Average Measured T_{op}, K	Average Weather During Obsrv.	Computed T_{atm}, K	Computed L_{atm}, ratio	Physical WG Temp., deg C	T_{wg}, K	Normalized[a] T_{op}, K
F1	10/13/90 DOY 286 0046-0122 UT	92.1[b]	894.1 mb 22.8 °C 12.09% RH	6.83	1.0256 (0.1097 dB)	22.8	17.85	92.1
F1	10/14/90 DOY 287 0700-0800 UT	92.0	892.0 mb 19.9 °C 19.0% RH	7.62	1.0286 (0.1225 dB)	23.6	17.89	91.2
F1	01/11/91 DOY 011 0006-0900 UT	93.9	901.7 mb 5.2 °C 72.8% RH	9.56	1.0368 (0.1570 dB)	8.6	16.99	92.2
F2	01/16/91 DOY 016 0330 UT	97.45[c]	893.8 mb 11.6 °C 34.4% RH	7.98	1.0304 (0.1299 dB)	19.7	17.66	96.6
F2	01/17/91 DOY 017 1730-1832 UT	97.53[d]	902.9 mb 10.0 °C 28.5% RH	7.21	1.0274 (0.1176 dB)	18.4	17.58	97.4
F3	11/11/90 DOY 315 0300-0800 UT	102.2	901.5 mb 17.3 °C 15.5% RH	6.76	1.0255 (0.1095 dB)	20.7	17.72	102.4
F3	12/18/90 DOY 352 1200-1700 UT	102.0	896.1 mb 5.5 °C 31.6% RH	6.69	1.0256 (0.1099 dB)	17.4	17.52	102.5
			After mirrors and ellipsoid realigned on 91 DOY 018					
F3	01/23/91 DOY 023 0400-0500 UT	98.5	895.7 mb 6.3 °C 20.3% RH	5.97	1.0229 (0.0981 dB)	21.3	17.75	99.4
F3	01/25/91 DOY 025 0530-0600 UT	98.2	896.1 mb 8.0 °C 33.4% RH	7.22	1.0276 (0.1181 dB)	22.2	17.81	97.9
F3	01/30/91 DOY 030 0330-0600 UT	97.1	899.2 mb 4.1 °C 13.8% RH	5.40	1.0207 (0.0891 dB)	20.7	17.72	98.6

[a] Normalized T_{op} values were computed through the use of Eq. (1).

[b] Average zenith values during tipping curve tests.

[c] Extrapolated from 3C84 STAR track off source at 83.76 deg elevation.

[d] From rise-set tipping curve data at 120 and 50 deg azimuth.

Table 4. Measured and computed zenith atmospheric noise temperatures at Ka-band (32.0 GHz)

Config.	Azimuth Angle, deg	Observation Period	Average Weather	Computed L_{atmz}, ratio	L^{a}_{ant}, ratio	Meas. $T_{op}(30) - T_{op}(90)$, K	Meas.[b] T_{atm}, K	Computed[c] T_{atm}, K	ΔT_{atm}, K
F1	50.0	10/12/90 DOY 285 1746-1822 UT	894.1 mb 22.8 °C 12.1% RH	1.0256 (0.1097 dB)	1.0932 (0.387 dB)	8.11	8.92	6.83	2.09
F3	50.0	11/12/90 DOY 316 2213-2236 UT	901.4 mb 22.5 °C 13.8% RH	1.0270 (0.1158 dB)	1.1397 (0.568 dB)	8.46	9.69	7.22	2.47
F2	120.0	01/17/91 1991 DOY 17 1730-1800 UT	902.8 mb 9.8 °C 29.5% RH	1.0277 (0.1186 dB)	1.1155 (0.475 dB)	8.92	10.00	7.26	2.69
F2	50.0	01/17/91 1991 DOY 17 1803-1835 UT	902.9 mb 10.0 °C 28.0% RH	1.0273 (0.1169 dB)	1.1155 (0.475 dB)	9.01	10.10	7.16	2.94
			After mirrors and ellipsoid realigned on 91 DOY 018						
F3	50.0	01/23/91 1991 DOY 23 1705-1748 UT	898.1 mb 9.3 °C 21.3% RH	1.0244 (0.1046 dB)	1.1226 (0.502 dB)	7.12	8.04	6.39	1.65

[a] See Eqs. (19) through (21).

[b] See Eq. (18).

[c] Computed values obtained from computer program SDSATM7M.BAS.

Table 5. Ka-band test package performance characteristics

Parameter	Performance Achieved
Receive polarization	Right circular polarization, left circular polarization (if reconfigured)
Receive frequencies	31.865–32.085 GHz determined from laboratory tests
T_{op} for test package on ground at DSS 13, zenith clear sky	85 K[a]
Measured T_{op} resolution for the above T_{op}, τ = 1 sec, 100 MHz bandwidth	< 0.06 K
Gain stability over 0 to 40 deg C ambient temperature range	< 0.2 dB peak-to-peak, < 0.05 dB/hr (thermoelectric temperature control)
Total calibration nonlinearity error	< 2%
Radio source temp. T_s measurement accuracy (T_s is obtained from a Δ measurement)	$\pm[0.06 + 0.020 \times T_s]$ K for $2 < T_s < 10$ K
Overall T_{op} measurement accuracy,[b] K $10 < T_{op} < 150$ K	< 0.8 K peak-to-peak

[a] A major part of the total is due to 56.6 K from the HEMT and 17.7 K from waveguide losses.

[b] Based on error analysis, calibration errors, and estimated mismatch errors.

Fig. 1. The new constructed BWG antenna.

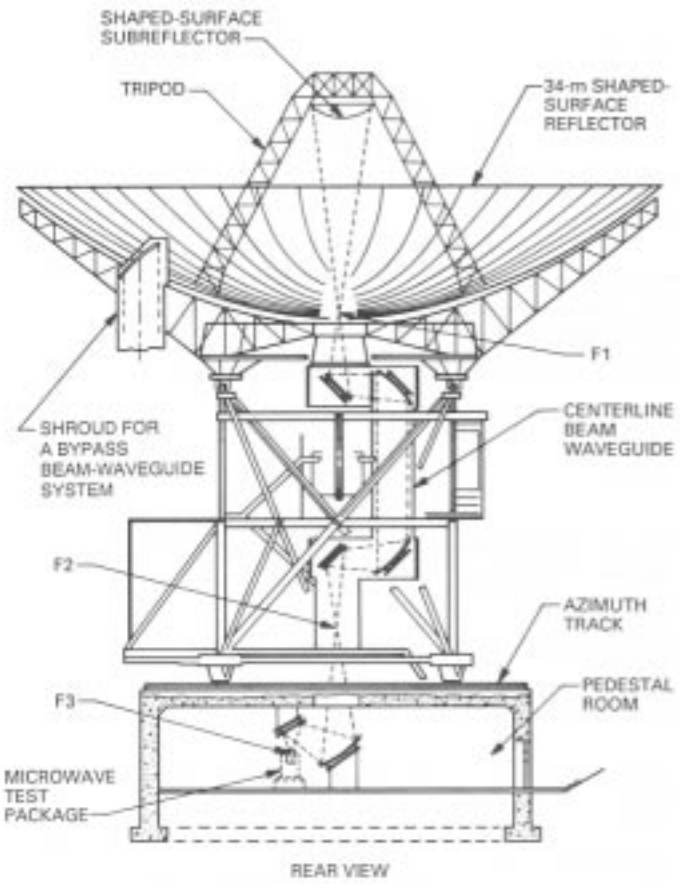

Fig. 2. The BWG antenna shown with focal points F1, F2, and F3.

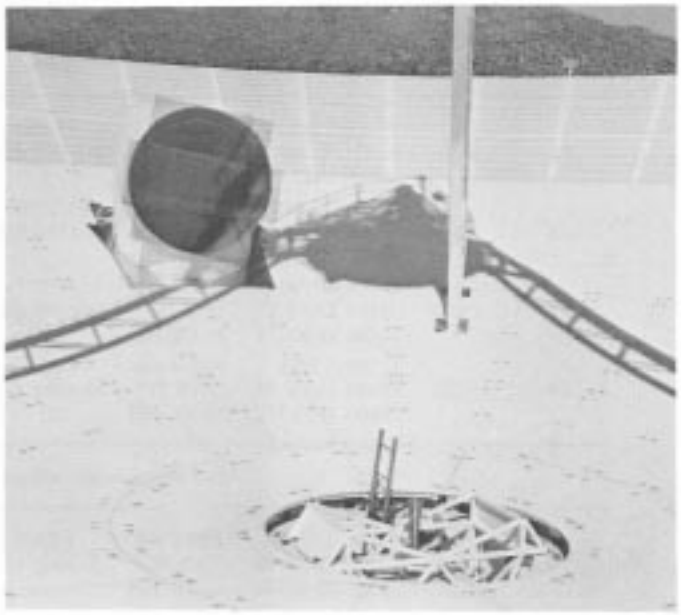

Fig. 3. Ka-band 29-dBi horn test package and mounting assembly installed at F1.

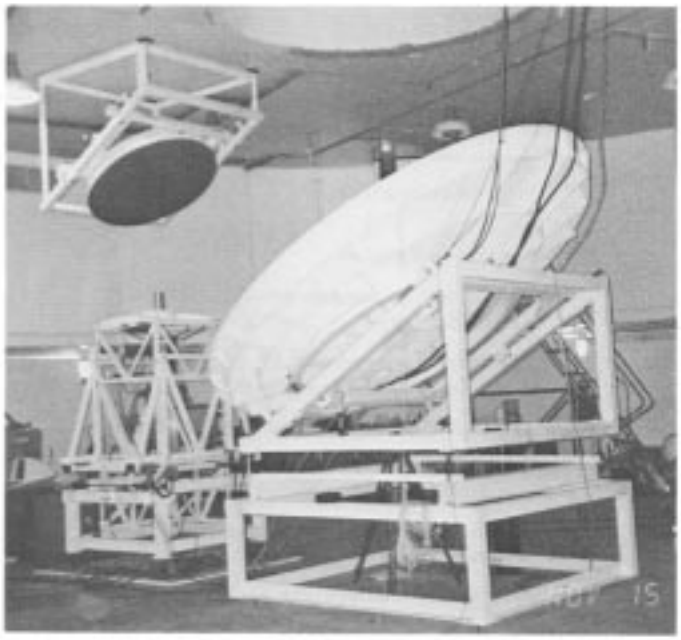

Fig. 4. Ka-band 23-dBi horn test package and mounting table installed at F3.

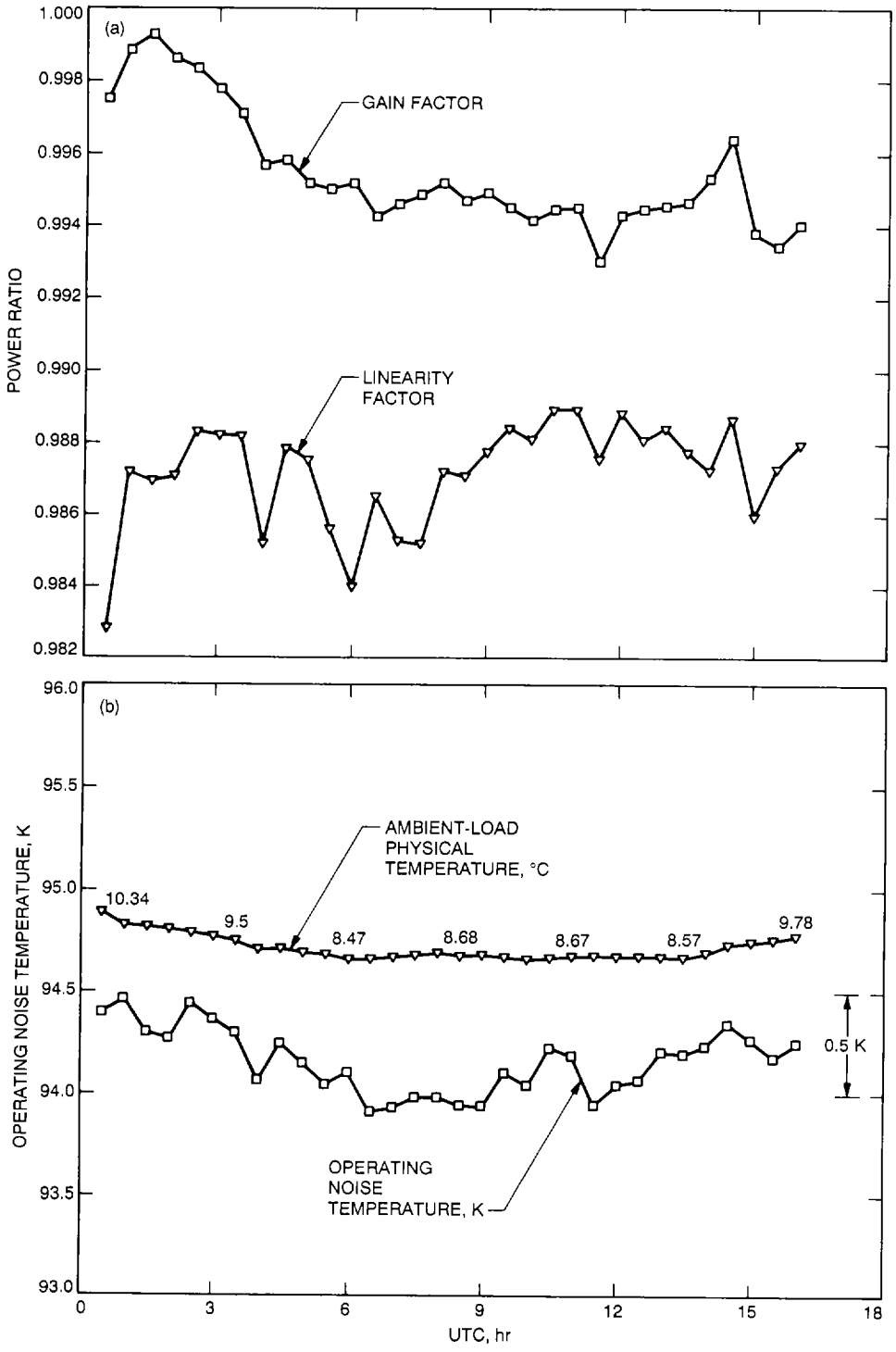

Fig. 5. Mini-cal data taken on January 11, 1991, with the Ka-band 29-dBi horn test package mounted at F1: (a) gain factor and linearity factor and (b) operating noise temperature and ambient load temperature.

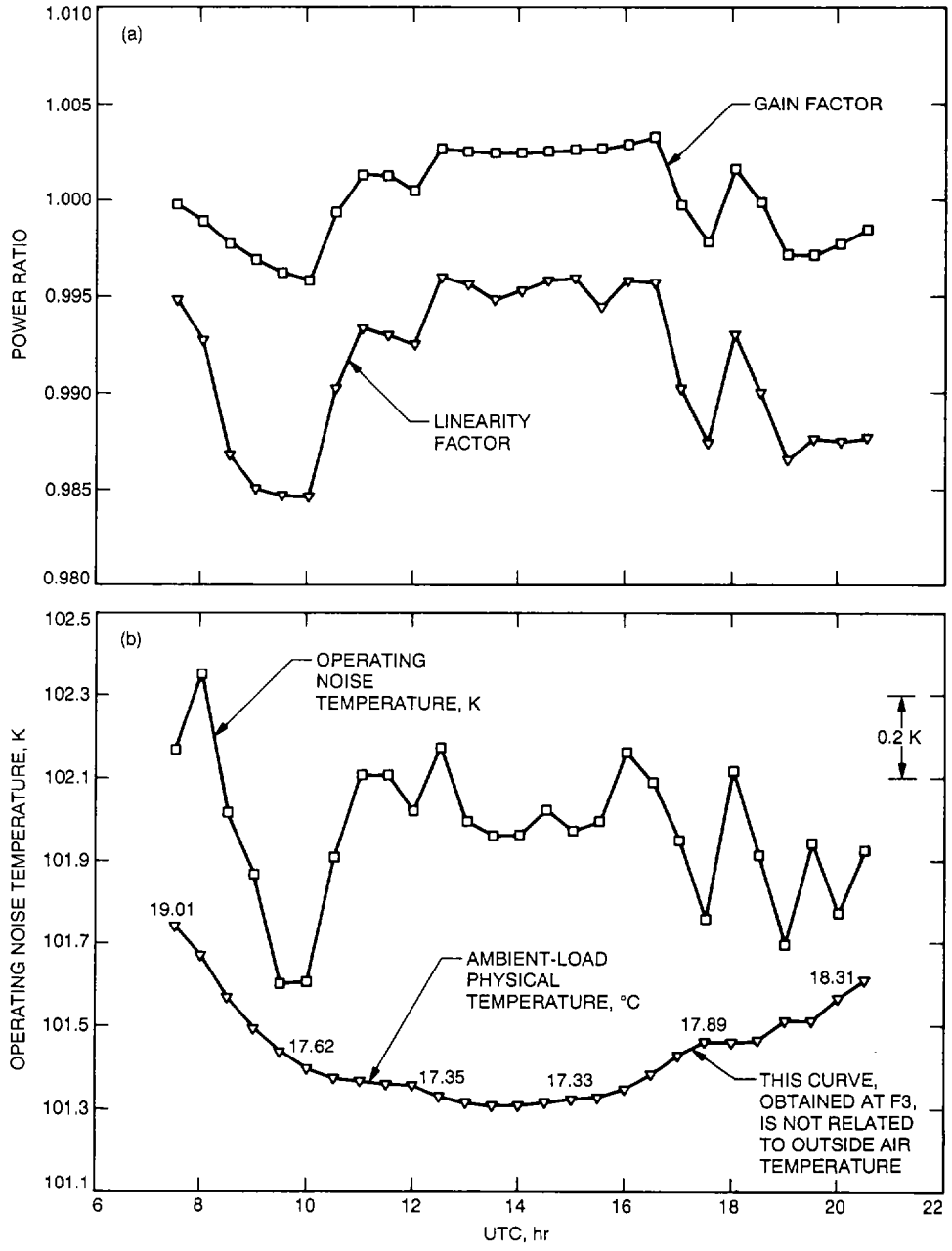

Fig. 6. Mini-calibration data taken on December 18, 1990, with the Ka-band 23-dBi horn test package mounted at F3: (a) gain factor and linearity factor and (b) operating noise temperature and ambient load temperature.

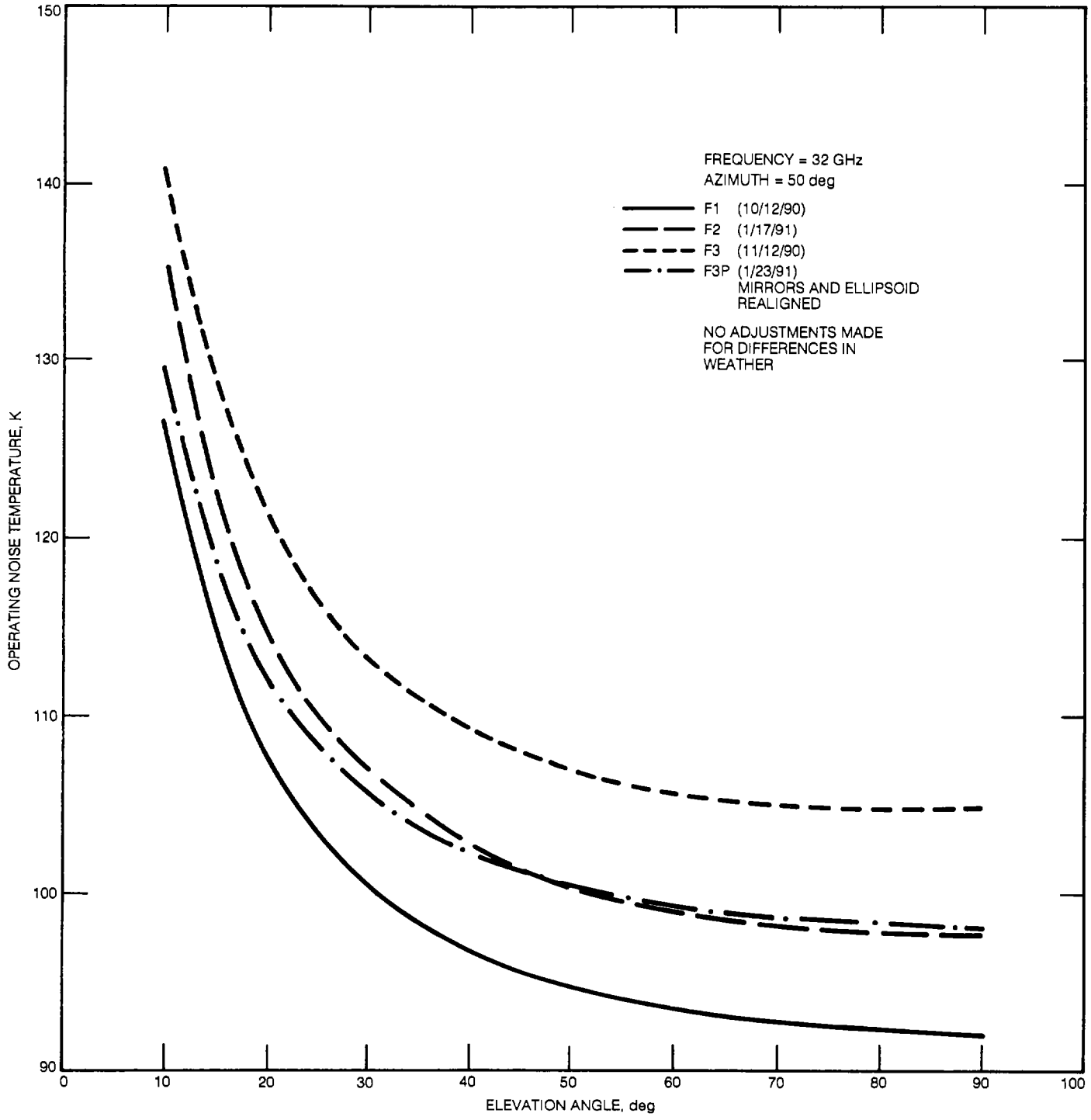

Fig. 7. Ka-band (32 GHz) tipping curves at F1, F2, and F3.

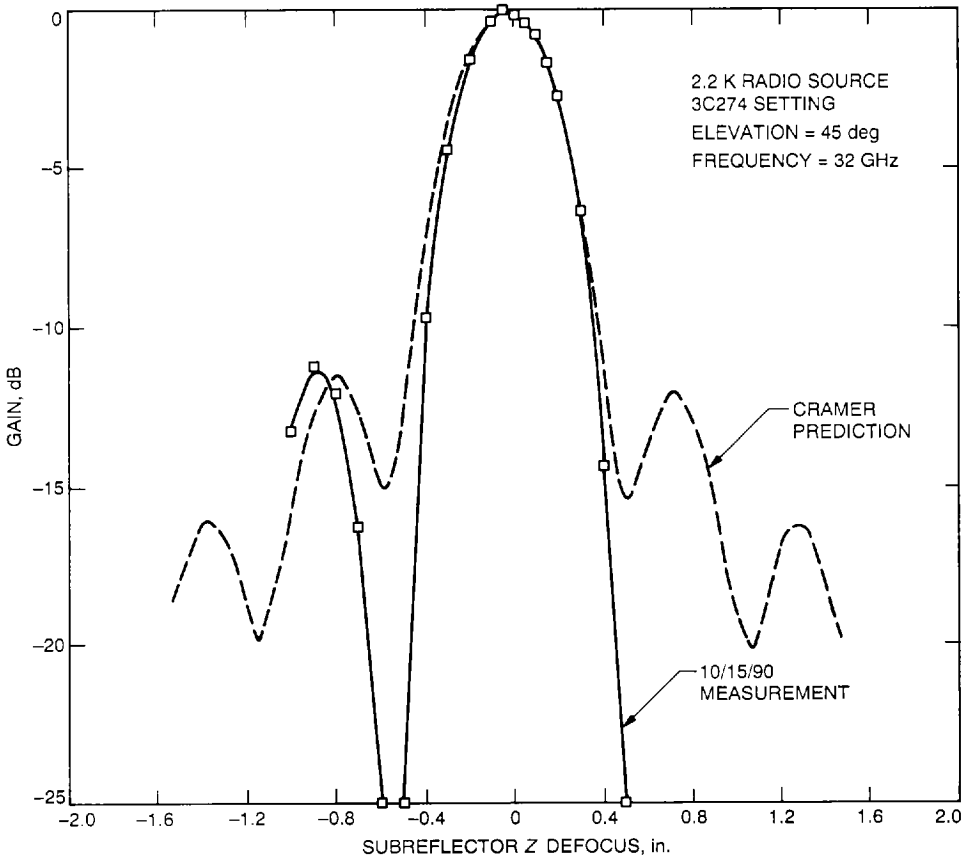

Fig. 8. Ka-band (32 GHz) subreflector *Z*-defocus curve measured at F1.

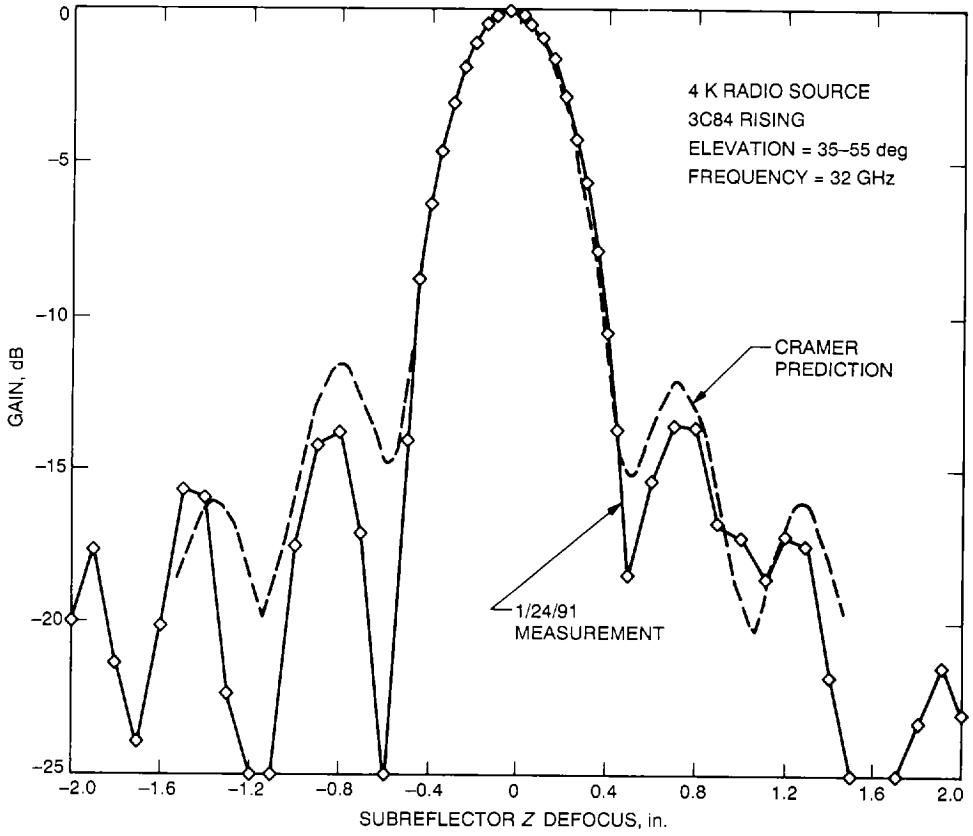

Fig. 9. Ka-band (32 GHz) subreflector *Z*-defocus curve measured at F3.

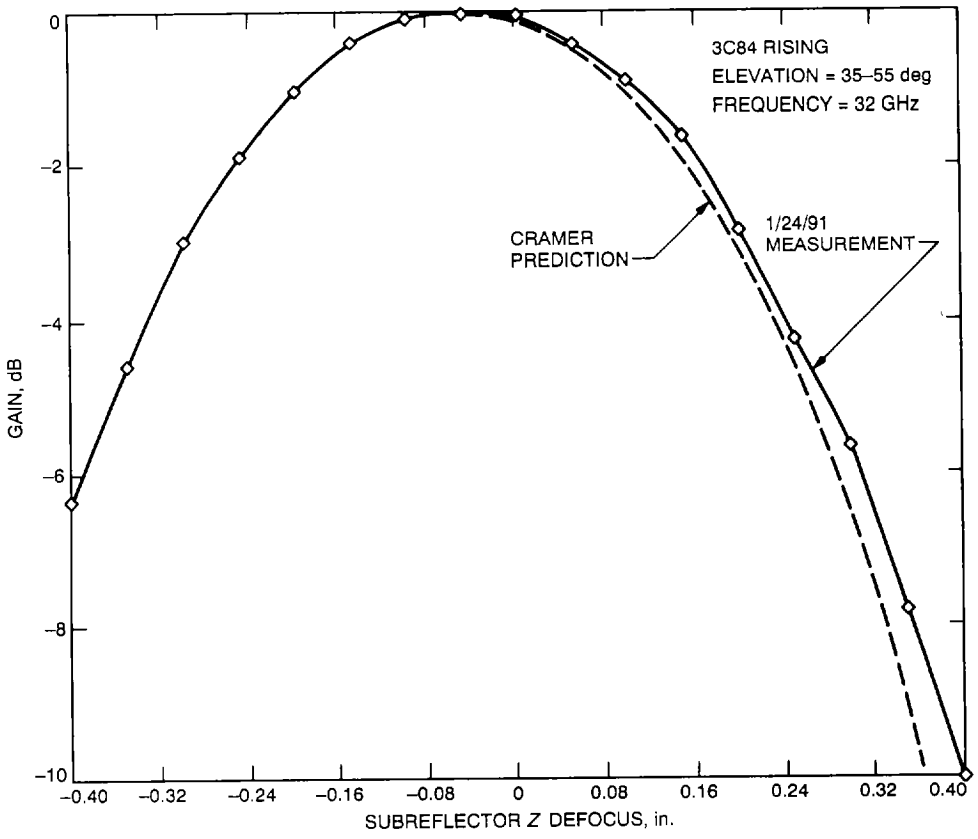

Fig. 10. Expanded detail of the main beam of the F3 Ka-band subreflector defocus curve (see Fig. 9).